https://doi.org/10.5194/tc-2020-123
Preprint. Discussion started: 7 May 2020

The Cryosphere Discussions

Spaceborne infrared imagery for early detection and cause of Weddell Polynya openings

Céline Heuzé[1] and Adriano Lemos[1]

[1]Department of Earth Sciences, University of Gothenburg, Gothenburg, Sweden

Correspondence: Céline Heuzé (celine.heuze@gu.se)

Abstract. When will sea ice open is a crucial information for navigation and scientific deployments. This became painfully obvious when the Weddell Polynya, a large hole in the winter Southern Ocean sea ice, unexpectedly re-opened in 2016 for the first time in forty years. With no early warning, observations were limited to chance autonomous sensors, so the much-debated cause of the opening still cannot be determined accurately. We aim here to create such an early warning system. From the full historical sea ice concentration record, we find in fact 30 polynyas since 1980. Then, using the full time series of the spaceborne infrared Advanced Very High Resolution Radiometer, we determine that these events can be detected in the two weeks before the polynya opens. Area-average median brightness temperature larger than 253 K in all three bands and area-maximum larger than 269 K along with a footprint at least larger than 4000 km^2 successfully forecasts the polynyas and does not return any false positive. Or rather, it returned false positives that were in fact events that the sea ice concentration threshold had missed. Moreover, we find temporal oscillations in brightness temperature that could indicate upwelling of warm water, but also changes of sign in T45 (band 4 – band 5) which could indicate a lead. We hence combine the spaceborne infrared data with atmospheric reanalysis, hydrographic mooring data and Sentinel-1 radar imagery and find that all events, including the 2017 Weddell Polynya, are caused by both atmospheric divergence and oceanic upwelling. That is, the debate is closed: both parties are correct; the Weddell Polynya is a hybrid.

1 Introduction

Global changes in the sea ice cover, of which the continuous decrease in summer Arctic sea ice since satellite observations began in the 1970s is the most dramatic example (Stocker et al., 2014; Notz and Stroeve, 2016), lead to a development in commercial exploitation of ice-infested waters in both hemispheres (Meier et al., 2014; Schillat et al., 2016). For planning purposes and for navigation, early detection of sea ice opening is urgently needed. Polar researchers would also benefit from such product. In 2016, the most famous opening in the Antarctic sea ice, the Weddell Polynya (Carsey, 1980), re-appeared for the first time in forty years (Swart et al., 2018). Luckily, two autonomous profilers were drifting over the polynya region as it was opening (Campbell et al., 2019), but these are the only data ever collected during one of its openings. An early-warning

https://doi.org/10.5194/tc-2020-123
Preprint. Discussion started: 7 May 2020

system, even if it is but a few days, would allow for potentially re-routing autonomous sensors or nearby expeditions and hence obtaining such precious data.

Polynyas are holes formed in the winter pack ice in both hemispheres, by the coast or offshore (Morales Maqueda et al., 2004; Smith Jr et al., 2007). By suddenly exposing the comparatively warm ocean to the cold winter atmosphere, they have a large impact on the entire climate system: they modify the whole water column (Gordon, 1978), contribute to deep water formation (Martin and Cavalieri, 1989) and hence impact the global ocean circulation (Heuzé et al., 2015a), and may be responsible for the observed warming of the deepest waters (Zanowski et al., 2015). Moreover, the vertical motion of water that they trigger ventilates the deep ocean and brings nutrients up, making polynyas a biological hotspot (Smith Jr et al., 2007). The largest of them all, the Weddell Polynya or Maud Rise Polynya, opens in austral winter in the Weddell Sea sector of the Southern Ocean. Until 2016, it had been observed only once, at the beginning of the satellite era in winters 1974-1976, when it reached a maximum area of 350 000 km^2 (Carsey, 1980). Although there was no Weddell Polynya in the following 40 years, a "halo" of low sea ice concentration did regularly appear in the region (Lindsay et al., 2004; Smedsrud, 2005; de Steur et al., 2007), suggesting that the process that caused the polynya was still at play. The exact process is still debated though, owing to the lack of in-situ data. The many hypotheses fall into two broad categories:

- the atmospheric argument is based on relationships between the polynya and the strength or persistence of the Southern Annular Mode, or the strength of the wind itself (e.g. Cheon et al., 2014; Francis et al., 2019; Campbell et al., 2019)
- the oceanographic argument is two-fold: that the Maud Rise region is weakly stratified, hence prone to deep convection and polynya events (Kjellsson et al., 2015; Heuzé et al., 2015b; Wilson et al., 2019), and that the polynya opens when comparatively warm Circumpolar Deep Water is upwelled (Holland, 2001; Martin et al., 2013; Dufour, 2017; Cheon and Gordon, 2019).

The lack of in-situ data could be compensated by satellite-based observations. The most common method to monitor sea ice globally consists in daily estimates of sea ice concentration from passive radiometers or spectrometers (Spreen et al., 2008), mostly in the microwave region (e.g. AMSR-2 frequency of 89 GHz, or wavelength of approx. 3 mm). Passive microwave is also commonly used for the determination of sea ice age (Korosov et al., 2018), a proxy for its thickness and salinity. Microwave products have a relatively low horizontal resolution of the order of 3 km, so (active) Synthetic Aperture Radar (SAR) has become the norm for high resolution applications such as lead (Murashkin et al., 2018) or melt pond detection (Mäkynen et al., 2014), sea ice drift tracking (Demchev et al., 2017), classification (Aldenhoff et al., 2018) and especially thickness retrievals (e.g. Zhang et al., 2016). To the best of our knowledge, none of these methods has been used for detecting that sea ice is about to open. Moreover, both microwave and SAR are comparatively recent sensors (Drinkwater, 1998). In contrast, spaceborne infrared imagery has been used to monitor sea ice since the late 1970s from multi-mission satellites, which gives a higher-than-daily coverage and makes it a quite robust method (Comiso, 1991). Spaceborne infrared is very sensitive to clouds, and hence has fallen out of fashion for polar research (Drinkwater, 1998). However, the preliminary study of Heuzé and Aldenhoff (2018) suggests that the upwelling and/or heat loss to the atmosphere caused by sea ice thinning prior to the Weddell Polynya opening might be detectable in infrared data.

https://doi.org/10.5194/tc-2020-123
Preprint. Discussion started: 7 May 2020

We here investigate to what extent the nearly 40-year record of spaceborne infrared imagery can be used both for potential early detection of upcoming re-opening of the sea ice, but also to determine the mechanisms that cause the sea ice to open. After detailing our processing in section 2, in particular the cloud masking, we start by verifying how many polynya events have occurred since records began (section 3.1) and their respective starting dates. We then determine criteria on the infrared brightness bands that successfully detect all these events and minimise the amount of false positives (section 3.2). Finally, as the infrared time series can also show whether the polynya opened from a lead or from upwelling, we further investigate the events for which we have in-situ data in the vicinity, including the much-debated 2017 Weddell Polynya (section 3.3).

2 Data and Methods

2.1 Data

In this study, we first determine the dates of past polynya events since 1980 using spaceborne microwave-based sea ice products as reference. We then study these events using spaceborne infrared data, validated against in-situ hydrographic data and atmospheric reanalyses, but also SAR imagery. Our region of interest (red contours on Fig. 1), hereafter referred to as "the polynya-prone region", lies over the topographic feature Maud Rise, in the eastern Weddell Sea sector of the Southern Ocean (longitude 6° W to 12° E; latitude 68° S to 60° S).

For reference, we use daily sea ice concentration at 25 km resolution from the National Snow and Ice Data Center, available continuously since 1978 (Cavalieri et al., 1996). We also briefly use in section 3.2 the higher resolution sea ice concentration product from the University of Bremen (Spreen et al., 2008), available since 2002.

The spaceborne infrared data come from the Advanced Very High Resolution Radiometer (AVHRR) Polar Pathfinder or APP, provided by the National Oceanographic and Atmospheric Administation (Key et al., 2019). It provides twice-daily, 5 km gridded composites of all available AVHRR brightness temperature data since 1982. We use only the ones acquired at 2 AM to ensure that we work year-round with dark images. The three bands that we use are commonly referred to as T3b (wavelength of 3740 nm), T4 (10800 nm) and T5 (12000 nm).

For validation, we use the hourly 2 m temperature and 10 m horizontal wind components u and v from the European Centre for Medium-Range Weather Forecasts ERA5 hourly reanalysis, provided on a 0.25° grid (doi: 10.24381/cds.adbb2d47). Hydrographic data come from three moorings deployed since 1996 along the Prime Meridian by the Alfred Wegener Institute, named AWI229 (Fahrbach and Rohardt, 2012a; Rohardt and Boebel, 2019), AWI 230 (Fahrbach and Rohardt, 2012b, c) and AWI 231 (Fahrbach and Rohardt, 2012d). Finally, we also use the backscatter information from Sentinel-1 SAR images in the extra-wide swath mode (approx. 40 m resolution) provided by the European Space Agency / Copernicus. We use only the HH polarisation, as we do not perform a detailed analysis but rather a qualitative assessment of sea ice conditions.

https://doi.org/10.5194/tc-2020-123
Preprint. Discussion started: 7 May 2020

The Cryosphere Discussions
Open Access
EGU

2.2 Cloud masking of APP data

Clouds are a known issue for AVHRR data, especially in polar regions (e.g. Drinkwater, 1998). The first cloud filters adapted to the polar regions were designed by Yamanouchi et al. (1987), which imposed criteria on T4, T34 (T3b minus T4) and T45 (T4 minus T5) to detect thick, high and thin clouds, respectively. Saunders and Kriebel (1988) added a geographical/texture perspective, imposing criteria on 3 by 3 pixel areas, while Key and Barry (1989) added a temporal perspective, comparing each pixel from day to day. But these filters did not perform as well as expected, and we had to wait until Vincent et al. (2008) for extra criteria on T45 that can detect ice fog.

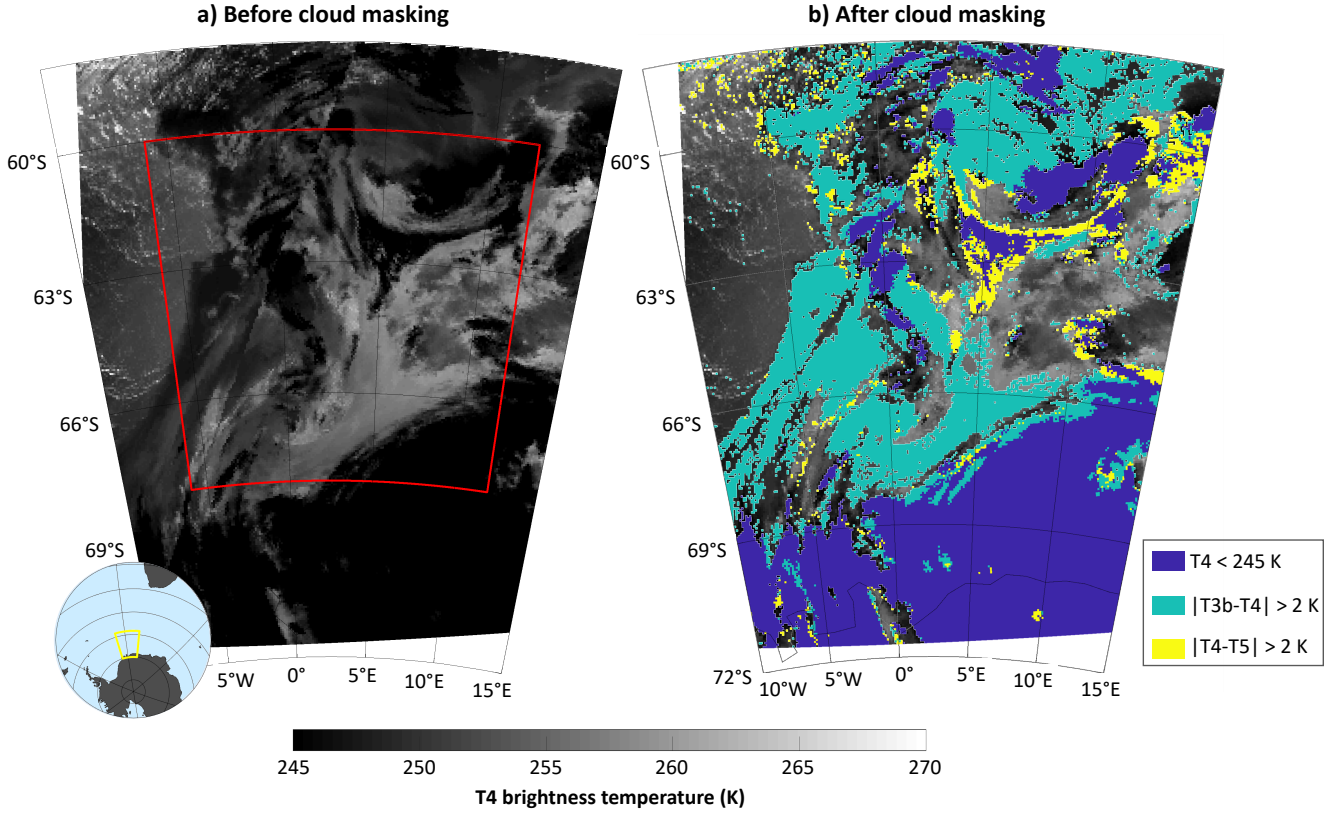

Figure 1. Brightness temperature T4 from APP (provided by NOAA, Key et al., 2019) on 1 September 2017 before (a) and after (b) cloud masking. Colours indicate the different masking criteria from Yamanouchi et al. (1987, indigo and green) and Vincent et al. (2008, yellow). Insert indicates the location of the two images. Red contours on panel a, the location of the so-called polynya-prone region that we use in this study.

We aim to create a system that can work on individual images independently, so the approach of Key and Barry (1989) is not adapted. Likewise, Saunders and Kriebel (1988) is mostly based on day-time images, so not for us. We hence use the following three criteria to detect clouds (Fig. 1):

https://doi.org/10.5194/tc-2020-123
Preprint. Discussion started: 7 May 2020

- T4 $<$ 245 K (indigo, Yamanouchi et al., 1987);
- or |T34| $>$ 2 K (green, Yamanouchi et al., 1987);
- or |T45| $>$ 2 K (yellow, Vincent et al., 2008)

As shown on Fig. 1, these criteria are not perfect, but visual verification (not shown) proves that they are powerful enough to detect most of the clouds. Moreover, leads and polynyas generate a large heat and moisture flux (e.g. Cheon et al., 2014), which we do not want to see masked as a cloud or else we will not detect the polynyas. Any pixel that meets any of the three criteria listed above is set to NaN in all three bands T3b, T4 and T5 for our calculations.

2.3 Methods

We first detect polynyas by applying sea ice concentration thresholds on each pixel, or on the area-average. We show only three different thresholds based on the literature in section 3.1 (Gloersen et al., 1992; Gordon et al., 2007; Campbell et al., 2019), but we tested and visually assessed each option between 15 and 100%. We calculate the area of the polynya by simply multiplying the number of contiguous pixels with sea ice concentration lower than the specific thresholds by the pixel area. An event is defined as an uninterrupted series of consecutive days with sea ice under that threshold (60% for most of the study); if there is a day with higher sea ice concentration in between, a new event is created.

The aim of our work is to eventually produce an automatic system that would be scanning the polynya-prone region, so we do not track individual polynyas and instead analyse the brightness temperature time series over the whole region in section 3.2. For robustness though, we did produce brightness temperature composites centered on each polynya, which yielded similar results (not shown). For each day from 1982 to 2018, we produced time series of the geographical median, standard deviation, minimum and maximum brightness temperature over the polynya-prone region for each band, but also anomalies of these brightness temperatures relative to daily climatological values over the 40 years. Note that we produced a separate climatology using only the years with no polynya, but found no significant difference (not shown).

Finally, the atmospheric and hydrographic data used in section 3.3 are directly studied without further processing, except for the wind components. We produced over each polynya a time series of so-called curl of the wind. We cannot compute the wind stress curl per se, as we lack the drag coefficient, which will anyway change depending on whether the polynya is open or close. So instead, we use a similar method as e.g. Petty et al. (2016) and work with the curl of the wind components u and v:

$$curl = \frac{\partial v}{\partial x} - \frac{\partial u}{\partial y}. \quad (1)$$

We are not studying the actual values of that curl, only whether it is positive (suggesting divergence that could open a lead) or negative (suggesting an upwelling).

https://doi.org/10.5194/tc-2020-123
Preprint. Discussion started: 7 May 2020

3 Results and Discussion

3.1 Polynya dates

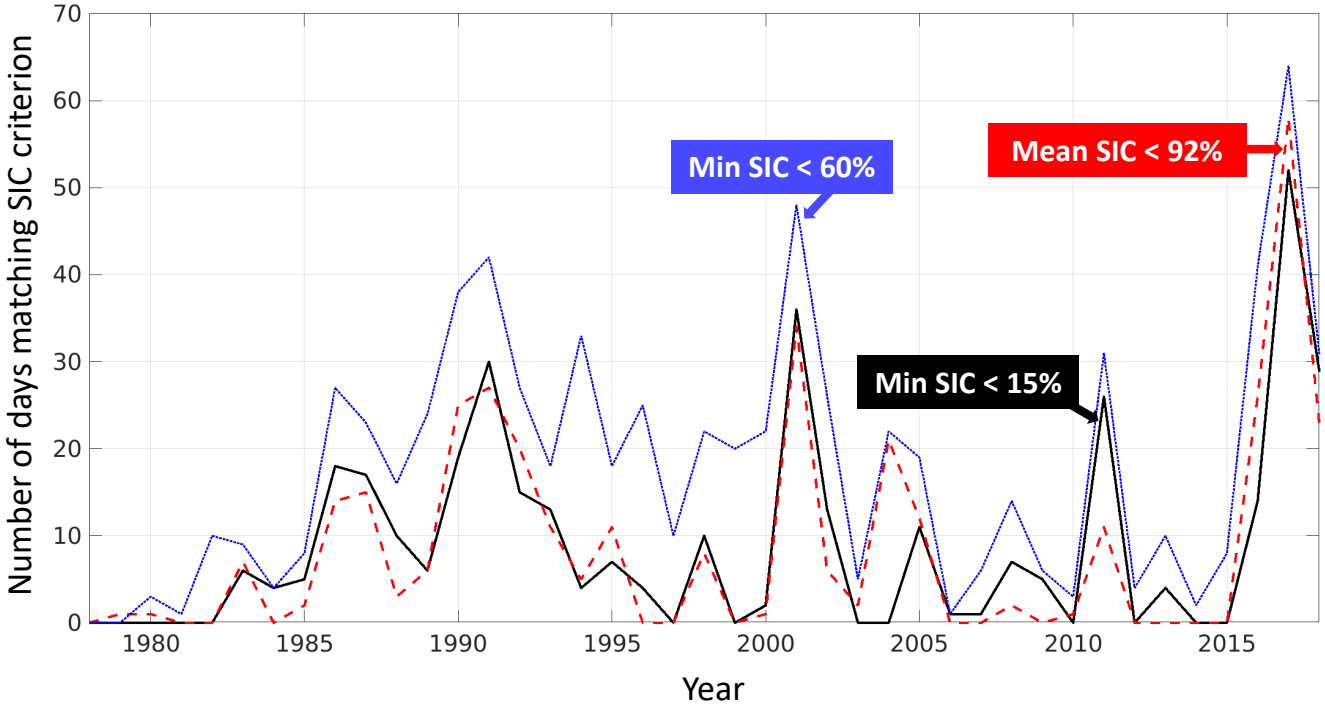

Figure 2. For each year of the NSIDC sea ice time series (1978-2018), number of days between 1st July and 31st October with a polynya according to the three most common criteria in the literature: black, minimum sea ice concentration (SIC) lower than 15% (e.g. Gloersen et al., 1992); blue, minimum sea ice concentration lower than 60% (Campbell et al., 2019); red, average sea ice concentration over the polynya-prone region lower than 92% (after Gordon et al., 2007).

We start by determining the dates of the polynya events that we want to further study, using the traditional criterion sea ice minimum over the region lower than 15% (black, Fig. 2) or lower than 60% (blue), and that of average sea ice concentration (SIC) lower than 92% (red). We limit ourselves to the period 1st July to 31st October. As noted by Campbell et al. (2019) already, these methods return qualitatively similar results; it is only the number of days with each criterion that differ. They all agree there was some polynya activity in the late 1980s - early 1990s and early 2000s, the so-called Maud Rise halo already studied notably by de Steur et al. (2007). Then, the region was rather quiet until the widely reported 2016-2017 return of the polynya (Swart et al., 2018).

The 60% criterion represented by the blue line probably includes late freeze-up or early melt events. The actual method used by Campbell et al. (2019) does not use fixed dates for winter, but rather limits itself to the period that starts one week after the first 90% SIC and finishes one week before the last 90%. For consistency with the other methods, we used fixed winter dates

https://doi.org/10.5194/tc-2020-123
Preprint. Discussion started: 7 May 2020

for their criterion too. We then visually checked the individual images to separate such late freeze-up / early melt from the actual polynya events. This visual validation also showed that the 60% criterion performed best (not shown).

The characteristics of the events thus detected are given in appendix table A1. We have 24 events over 11 years, which yield 30 polynyas because 5 events have two to four polynyas in the region simultaneously. In the case of the first such double in 1996, the two polynyas quickly merged. In October 2004 in contrast, there are originally two polynyas (a large one in the south; a smaller one in the north-east), then a third opens in the north-west on the same day the largest one splits into two! The now-two southerly polynyas close two days after, whereas the newly opened one in the north keeps growing and becomes the largest, ultimately absorbing the other one. Note that all durations make the polynya disappear on 1st November because of our end date criterion.

These thirty polynyas open at key locations in the region (Fig. 3). The maximum number of polynyas opening at the same grid cell, nine, is on the north-east flank of Maud Rise, with most of the others opening over Maud Rise or on its south-west flank. The central role of Maud Rise as shown by Holland (2001) is obvious. There is also a non-negligible number of grid cells in the southern part of our region with at least one opening. Unlike in models (e.g. Martin et al., 2013), Fig. 3 shows no opening over the open ocean.

3.2 Infrared-based early detection criteria

In the previous section, we determined the dates of 24 polynya events (giving 30 actual polynyas) from sea ice data dating back to 1978. We now investigate, in the timeseries of brightness temperature from APP, whether all these events share something in common, especially in the two weeks leading up to the event. We present the 30 days prior to the events in section 3.3 but we found that for the current purpose, 15 days are enough. As explained in the Methods section, this "something in common" needs to be easily detectable by a crude automatised system, hence we computed basic single-image properties over the entire polynya-prone region (Fig. 4): the geographical median, standard deviation, maximum and minimum. We analyse the range of their values in the 15 days leading to the event (one point per event on Fig. 4).

We want to find a criterion that would not only robustly detect a polynya, but also not flag any false positive. Fig. 4 shows that such criterion will have to be band-dependent. For T3b (cyan diamonds) and T5 (red stars) for example, the geographical minimum is of no use owing to its large spread across the events, whereas it is very specific for T4 (black circles). For T4 and T5, it is the standard deviation that is of no use: the 15-day minimum is always at 0, regardless of the event, and the maximum can also be 0. The geographical median and maximum look most promising, so we verify how many false positives would be returned by using their smallest values as a threshold (i.e. for the median for T5, either 243.1 or 252.6 K, see Fig. 4). There are 3443 days with infrared data that are between 1st July and 31st October in the years with no polynya event. For the individual bands, only the temporal maximum of the geographical median and the temporal maximum of the geographical maximum, in absolute values (left, top and bottom, y-axis, Fig. 4), that wrongly detect fewer than 1000 days. That is not good enough.

What Fig. 4 reveals is that we need sacrifice only one or two polynya events to be much more restrictive. More specifically, few polynya points have a geographical median lower than 253 K, and a geographical maximum that does not exceed 269 K (268 K for T5). Similarly for the daily anomalies, most of the geographical maxima exceed 18 K. Combining these three

https://doi.org/10.5194/tc-2020-123
Preprint. Discussion started: 7 May 2020

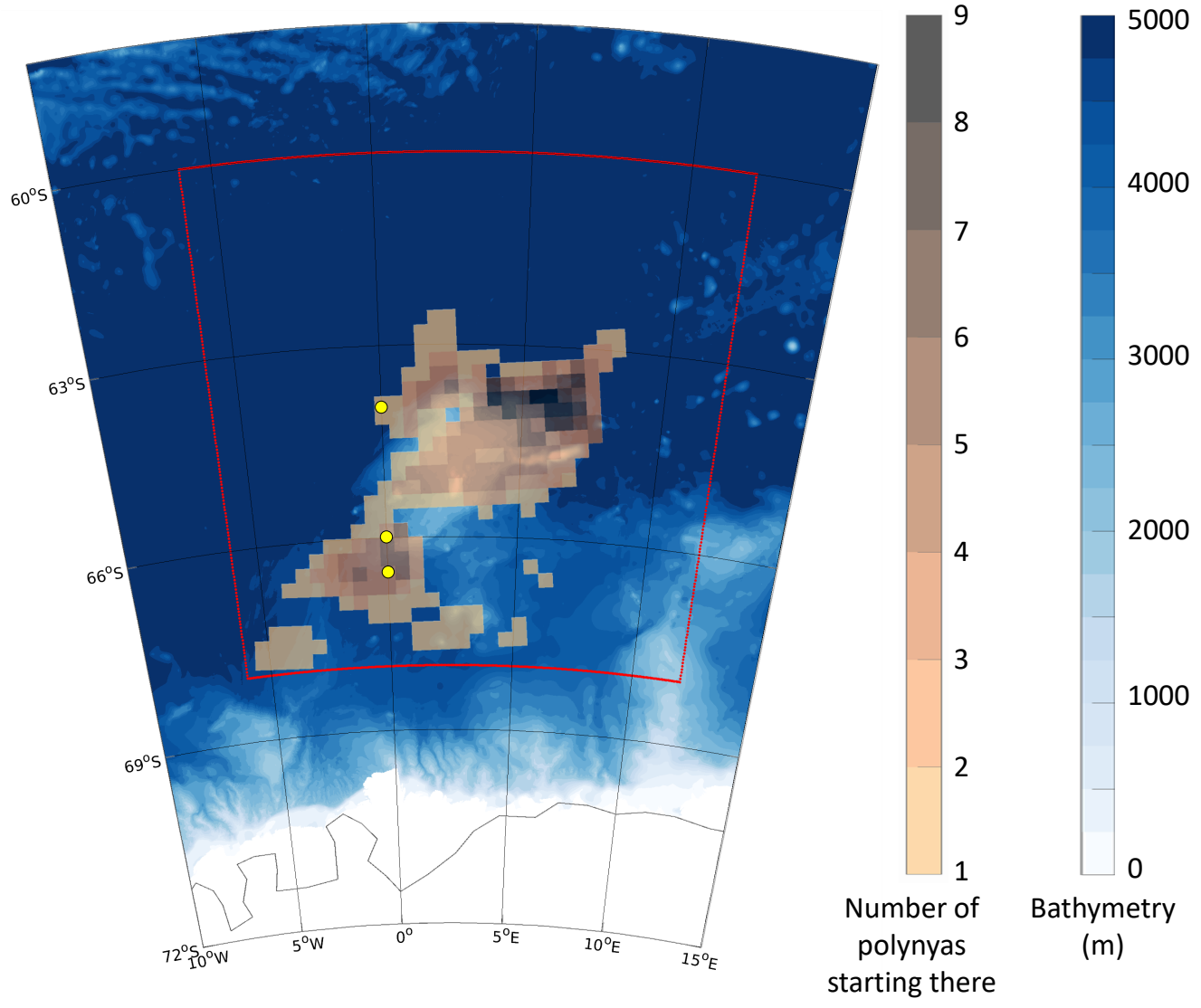

Figure 3. Out of the 30 polynyas detected, how many start at each location (transparent shading). Background: bathymetry of the region from GEBCO Compilation Group (2019). Red contours indicate our region of study for section 3.2, as in Heuzé and Aldenhoff (2018). Yellow dots mark the location of the three moorings used in section 3.3: AWI229 (north), AWI230 (middle) and AWI231 (south).

criteria, we obtain only 36 false positives. That is a remarkable improvement. We can also create an extra criterion based on the size of the signal detected: in our 24 polynya events, across the three bands, they all had on average more than 4000 km^2 of pixels affected. Note that we are not talking about the size of the polynya here, only the footprint on the brightness temperature data. If we add this final size restriction, we are left with 12 false positives (Table 1). But are they really false positives?

https://doi.org/10.5194/tc-2020-123
Preprint. Discussion started: 7 May 2020

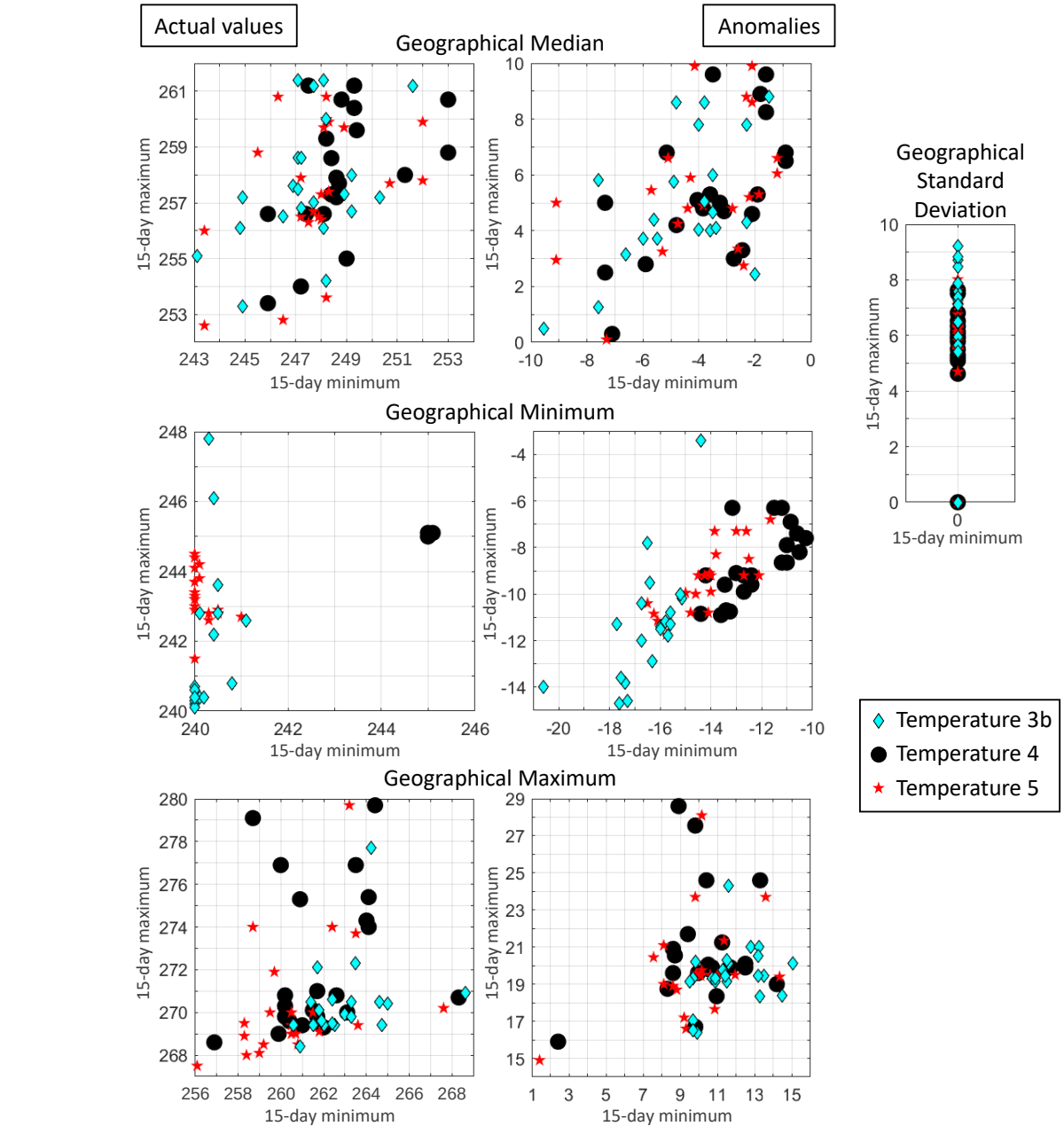

Figure 4. Over the polynya-prone region (red contours on Fig. 3), minimum (x-axis) and maximum (y-axis) over the time period from 14 days before the polynya opens until the day of opening of the geographical median (top), standard deviation (top right), minimum (centre) and maximum (bottom). One point per polynya event: cyan diamonds for the temperature band T3b; black circle for T4; red star for T5. Shown both the actual brightness temperature value (left) and the daily anomaly (right), both in degree K.

https://doi.org/10.5194/tc-2020-123
Preprint. Discussion started: 7 May 2020


The Cryosphere Discussions
Open Access
EGU

Table 1. For each false positive, i.e. day detected by our brightness temperature criteria but not by sea ice concentration criterion of section 3.1, minimum sea ice concentration in the polynya-prone region from low resolution NSIDC (prior to 2002) or higher resolution AMSRE from the University of Bremen (since Oct 2002). The last column provides further comments based on visual inspection.

Date	Min SIC	Comments
10 Oct 1982	81 %	Halo
12 July 1983	0 %	Late freeze-up
7 Oct 1984	85 %	Halo
13 July 1986	60 %	Late freeze-up
17 Aug 1986	71 %	Leads?
3 July 1987	0 %	Late freeze-up
31 Aug 1990	90 %	Halo
15 Sept 1997	90 %	Halo
20 July 1998	86 %	Halo
2 July 2001	0 %	Late freeze-up
18 Sept 2010	62 %	Halo or leads
22 Aug 2011	60 %	Tiny polynya

After visual examination, 4 of these false positives were late freeze-up. They all occurred in the first half of July, so a more restrictive winter date definition could solve this, potentially involving sea ice thresholds as in Campbell et al. (2019). Of the remaining 8, the majority had the typical halo appearance, with sea ice concentration between 60 and 90%. Some had even been mentioned in past publications (e.g. Smedsrud, 2005; Campbell et al., 2019), albeit with large uncertainties. The most obvious results were for the two latest dates, in 2010 and 2011, where we could verify the sea ice concentration at a much higher resolution in the University of Bremen datasets (Spreen et al., 2008). There, leads and small polynyas were directly apparent, proving the necessity of high resolution data for climate research. In summary, the criteria on the infrared brightness temperature did not return any false positive, or at least any that cannot easily be removed by simply checking the date. If anything, it successfully detected 8 extra events that the sea ice concentration criterion had missed.

We have completed our objective and determined brightness temperature thresholds to detect a polynya before it opens. Instead of stopping here, can we extract more information out of the infrared data? For example, an answer to the much debated "why did the polynya open"? One option is the difference between bands T4 (most adapted to ice) and T5 (most adapted to open ocean) or T45, where $T45 < 0$ means lead (Vincent et al., 2008). Unfortunately, out of the 24 events, all of them (Fig. 5a and supplementary Fig. A1) had a minimum T45 lower than 0 in the 14 days before the event. Which would mean that all of them had a lead somewhere in the polynya-prone region. The other option is that, as pointed out by Heuzé and Aldenhoff (2018), oscillations in the brightness temperature in the days before the polynya might reflect oceanic convective movements. The argument is that as the warm water is being upwelled, more heat is going through the ice; same as the ice thins, melted from below by that warm water. But likewise, all polynya events exhibit such oscillations, albeit with a frequency

https://doi.org/10.5194/tc-2020-123
Preprint. Discussion started: 7 May 2020

varying from 1 to 3 days depending on the band and event (Fig. 5b and c and supplementary Figs A2 and A3). In conclusion, we cannot determine the cause of the polynya opening from the infrared images alone. In the next section, we investigate this further, using in-situ validation data.

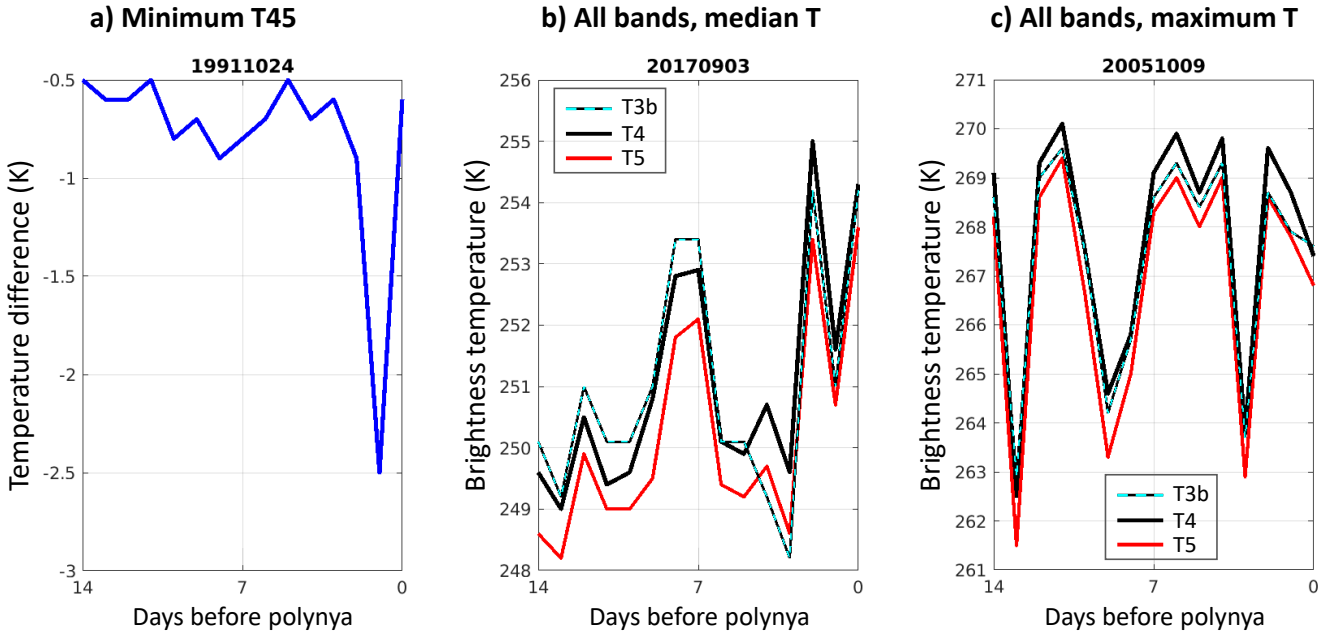

Figure 5. Example time series of geographical a) minimum brightness temperature difference T45 (T4 minus T5); b) median and c) maximum brightness temperature for all three bands, over the 14 days leading to the polynya event (date of the event in the panel title). For b) and c), thin dashed cyan line indicates T3b, thick black line T4, and red line T5. The figures with all events are given in the appendix.

3.3 Why did the polynyas open? An infrared-based discussion

There are two ways to open a polynya (Morales Maqueda et al., 2004):

- sensible heat / open ocean polynyas form when the sea ice is melted from below by the ocean. It requires that a comparatively warm water mass is upwelled, which should be visible in oceanic mooring data. A negative curl of the wind would indicate Ekman pumping, i.e. that the atmosphere is favourable to upwelling. Finally, positive air temperatures before the opening would contribute to the melting;
- latent heat / coastal polynyas in contrast form when the sea ice is pushed away by the wind. A positive curl of the wind would indicate such divergence.

From the infrared images, both mechanisms are possible: the oscillations in brightness temperature suggest an upwelling of warm water, but simultaneously a negative T45 suggests that leads open. We hence now augment our spaceborne infrared data with atmospheric and hydrographic data for clarification.

https://doi.org/10.5194/tc-2020-123
Preprint. Discussion started: 7 May 2020

The data coverage for the atmosphere is much better than for the hydrography, so we start with the atmosphere. The curl of the wind at the location of the individual 30 polynyas (listed in Table A1) alternates between negative and positive values for all polynyas (supp Fig. A4, negative curl / upwelling is blue, positive curl / divergence is red). That is, all polynyas have been preceded by both upwelling-prone and divergent winds. Note that the required timing is unclear: for divergence, e.g. Francis et al. (2019) says that it can open the ice within 12 hours, but to the best of our knowledge, no such specific value has been published for the upwelling.

The air temperature is not particularly helpful either, not least because we do not know what the melting point will be as we do not know the salinity of the sea ice or that of its snow layer. Nandan et al. (2017) puts an upper limit to 20 g/kg, which yields a freezing temperature of -1.1 °C (IOC, SCOR and IAPSO, 2010), and 0 °C if the sea ice is old and/or the snow layer fresh. Out of the 30 polynyas, 15 reach either of these freezing temperatures (supplementary Fig. A5). The main caveat here though is that the air temperatures are not given at the surface of the ice, but at 2 m height where it probably is colder. Moreover, these are reanalysis data, not actual observations at the polynya location, and hence are somewhat uncertain. All that we can say then is that three events remain colder than or around -10 °C, but for all the others it might have been warm enough to melt. Our conclusion for now is that the atmospheric reanalysis data did not provide a satisfactory discrimination.

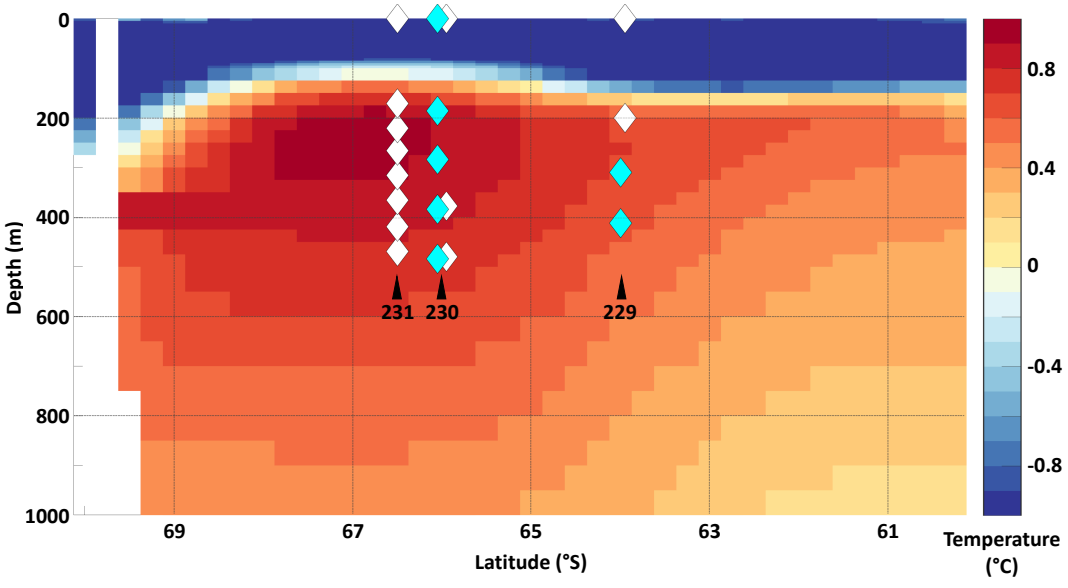

Figure 6. Climatological temperature along the Prime Meridian, from Locarnini et al. (2018), showing the comparatively warm Circumpolar Deep Water in red. The diamonds indicate the location of the mooring sensors used for our analysis; for moorings 229 and 230, white indicates the older deployment (229-5, in 2002-2005, and 230-2, in 1999-2000) and cyan, the more recent one (229-13, in 2016-2019, and 230-4, 2002-2005); for mooring 231, only deployment 231-5 (2002-2005) could be used here. Salinity section available as supplementary figure A6.

https://doi.org/10.5194/tc-2020-123
Preprint. Discussion started: 7 May 2020

We hence finish this paper with a more in-depth analysis of the three individual polynya events for which we have mooring data in the vicinity. Five mooring deployments coincide with a polynya event: one mooring (230-2) for 1999, three (229-5, 230-4, 231-5) for 2004, and one (229-13) for 2017. We want to determine if 1) we see in the mooring data upwelling of the comparatively warm and salty Circumpolar Deep Water (CDW), and 2) whether such upwelling is in sync with the brightness temperature oscillations. Unfortunately, for four out of five deployments, we are limited in the top 500 m to one sensor at the surface and all the others in the CDW (Fig. 6). We lack sensors in the top 100 m. Moreover, the surface sensor often had only temperature data, not salinity, and in the case of 229-13 for the 2017 polynya, there was no surface sensor data available; luckily, there were Sentinel-1 images. All we can study are variations in the CDW, both the suspected heaving of its core (Dufour, 2017) or its cooling as convection begins (Gordon, 1978). As sensors at the same depth returned different values but similar variability (not shown), we will not comment on the mooring values per se but only on their changes.

In 1999 (Fig. 7), the most notable variation is the dip in all infrared bands (panel a) and in T45 (panel b) 18 days before the polynya, mere hours after a warming and salinification of both deep sensors (panels e and f). The surface sensor (panel d) unfortunately shows variations that are of the level of the sensitivity of the instrument, and hence is not very useful. Then for two days, temperature and salinity at 480 m depth oscillate with a near 12 hour frequency, only to stop 13 days before the polynya, at the onset of the continuous increase in all infrared bands until 6 days before the polynya. Over that same period, the CDW depths cool down while the surface might be warming. All this seems to have started after a few hours of negative curl of the wind (panel c), suggesting that we might be witnessing an upwelling event from 13 to 7 days before the polynya. Finally, 4 days before the polynya, we see oscillations in all infrared bands and a strong negative T45. This immediately follows a sudden warming and salinification at 380 m depth (and to a lesser extent 480 m) before an intense cooling. In conclusion, in 1999, it seems that we first had upwelling 13 days before the polynya, convection starting 8 days before, and maybe leads 4 days before.

The 2004 event (Fig. 8) starts with a surprising decrease by 2 °C of the surface temperature 24 days before the event (panel d). All the other depths are rather stable until 18 days before the polynya, where they start having high frequency variability, especially at 170 and 220 m (panels e and f, respectively), correlated between salinity and temperature (warmer and saltier alternating with cooler and fresher). At the same time, the infrared brightness temperature in all bands oscillates while increasing to 260 K as average (panel a). Then starting 15 days before the polynya, the curl of the wind (panel c) becomes and stays negative for three days while the CDW oscillations continue and reach the deeper levels; to us, this obviously suggests upwelling. Following the lowest T45 of this series (-0.6 K, panel b) and divergent winds 11 days before the polynya, both the temperature at depth and the brightness temperatures increase again but without a change in salinity, which might indicate a lead. The final period in the two days before the polynya is more convincing: strong divergence in the wind, brightness temperature increases, but all depths see a cooling. We suspect that this indicates that a lead opened following the divergence, that the ocean is losing heat to the atmosphere, and that the infrared data detects that heat (and moisture) exchange to the atmosphere. Note that we showed only the mooring that had the most data, but all three moorings agree. For this event as well then, there might have been both leads and upwelling. Luckily for the last event that we will look at, radar images are available.

https://doi.org/10.5194/tc-2020-123
Preprint. Discussion started: 7 May 2020

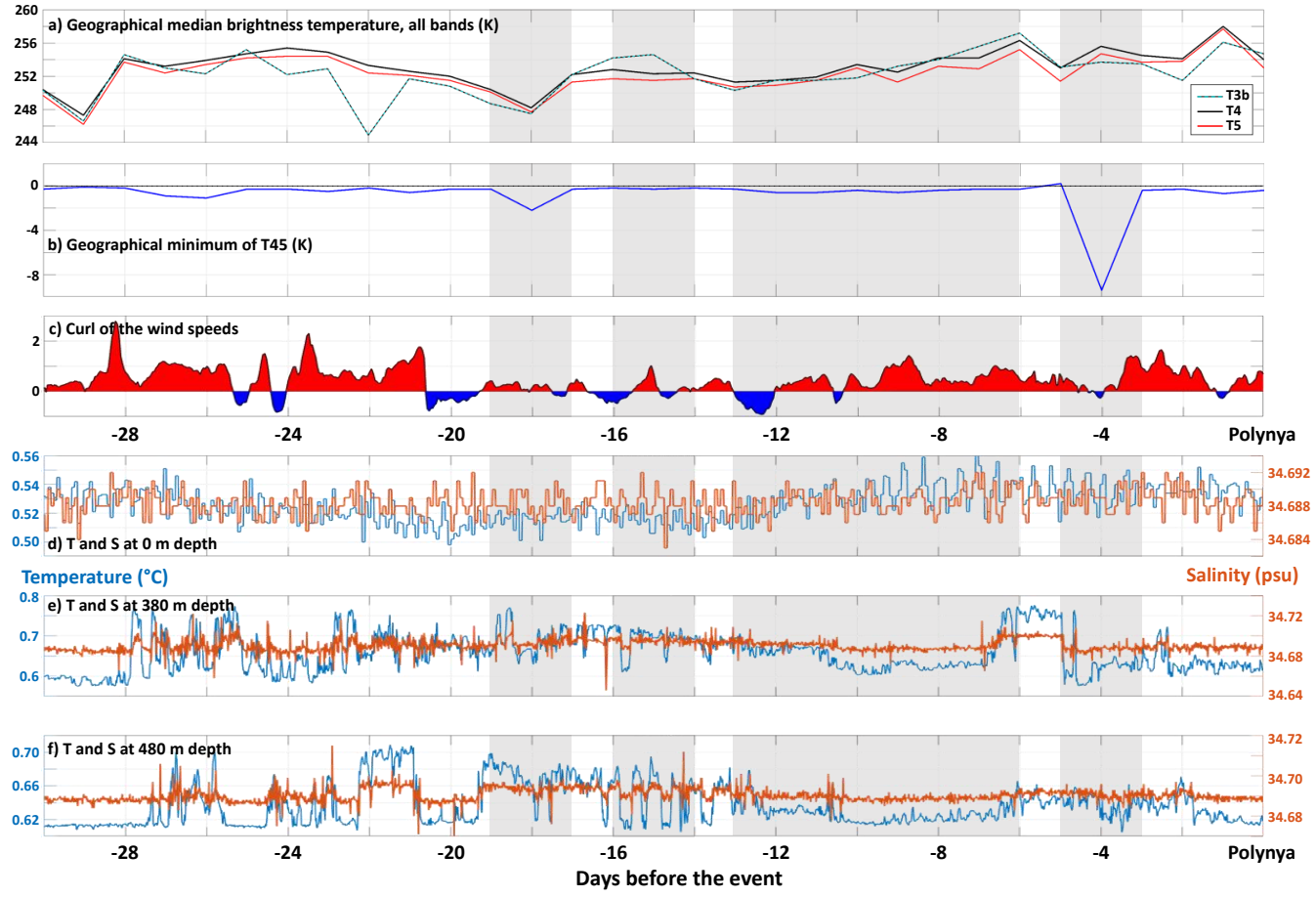

Figure 7. Conditions in the 30 days leading to the 24 October 1999 polynya. First, for the infrared criteria from section 3.2: a) geographical median over the polynya-prone region for the brightness temperature band T3b (cyan), T4 (thick black) and T5 (red); b) geographical min over the polynya-prone region of the brightness temperature difference T45 (T4 minus T5). c) curl of the wind speeds as in supp Fig. A4. Finally, temperature (blue) and salinity (orange) timeseries from mooring 230-2 (see Fig. 6) at 0 (d), 380 (e) and 480 (f) m depth. Grey boxes in the background highlight the time periods discussed in the text.

Finally, the 2017 event (Fig. 9) shows the same patterns again: an increase in variability along with a low T45 and divergent winds 15-14 days before the polynya (lead?), but also a synchronous increase in infrared brightness temperature and temperature and salinity at depth (upwelling?). But this time, we have high resolution Sentinel-1 SAR images to verify our hypothesis. What we see first is a sudden warming and salinification at depth from 19 to 16 days before the polynya (panels d and e). Straightafter, we again observe a decrease in T and S along with high frequency variability, just before the usual T45 lead signature (panel b); the ice is closed then on the SAR image. Five days later, or 11 days before the event, there are leads all around the area on the SAR image. One can imagine that the surface cooling resulting from the lead opening may have been strong enough to initiate convection, which would explain the apparent warming at 310 and 410 m. We see that three days later,

https://doi.org/10.5194/tc-2020-123
Preprint. Discussion started: 7 May 2020

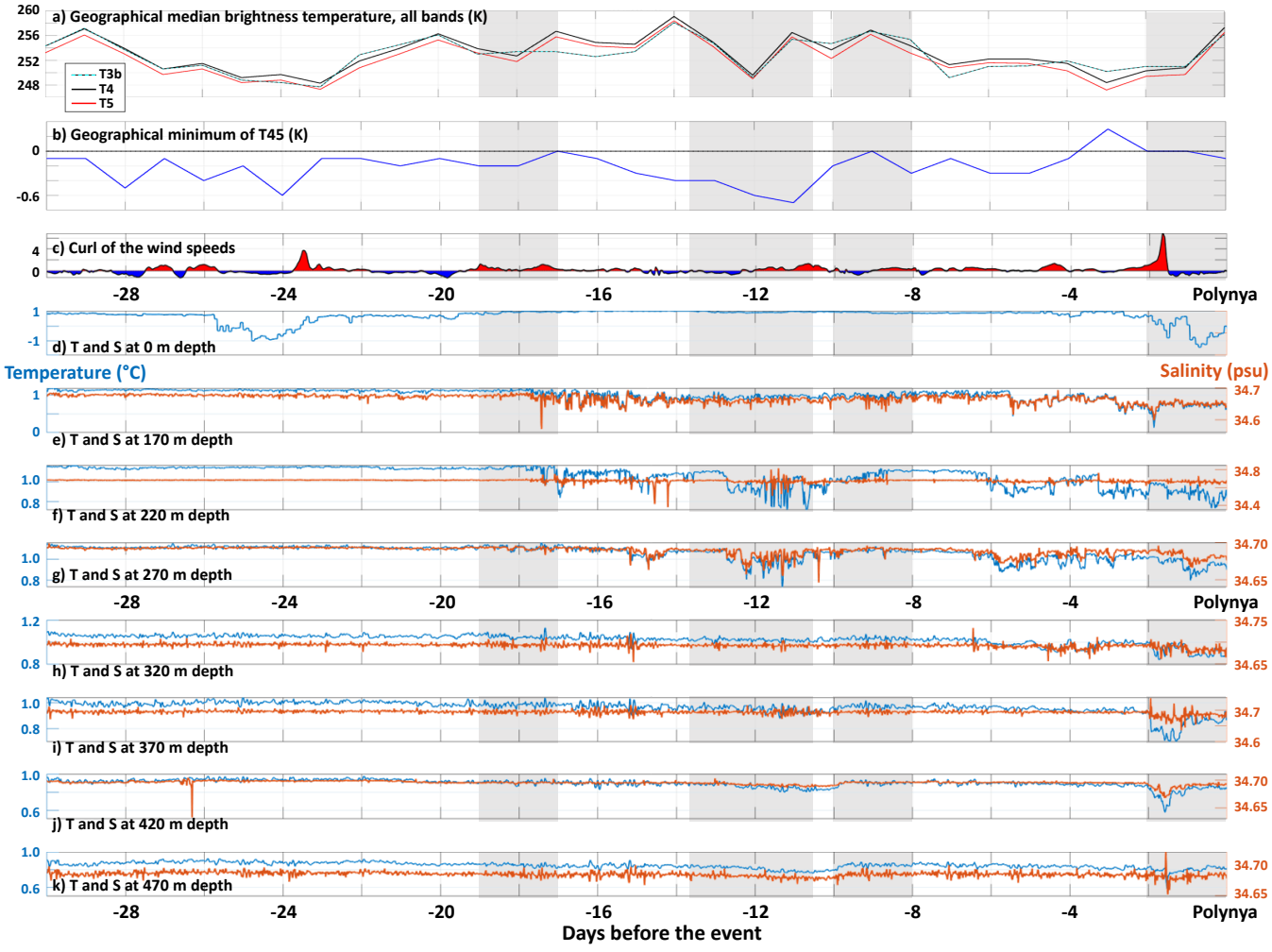

Figure 8. Conditions in the 30 days leading to the 9 October 2004 polynya. First, for the infrared criteria from section 3.2: a) geographical median over the polynya-prone region for the brightness temperature band T3b (cyan), T4 (thick black) and T5 (red); b) geographical min over the polynya-prone region of the brightness temperature difference T45 (T4 minus T5). c) curl of the wind speeds as in supp Fig. A4. Finally, temperature (blue) and salinity (orange) timeseries from mooring 231-5 (see Fig. 6) at 0 (d), 170 (e), 220 (f), 270 (g), 320 (h), 370 (i), 420 (j) and 470 (k) m depth. Grey boxes in the background highlight the time periods discussed in the text.

i.e. 8 days before the polynya, the leads have refrozen, so it is more likely is that the convection started as the ice formed again and ejected brine. The convection would bring down the cooled water from the surface to 310, 410 m depth, hence their cooling (as observed in reality and in models, Gordon, 1978; Smith Jr et al., 2007; Martin et al., 2013; Cheon and Gordon, 2019). And although we lack images between 8 and 4 days before the polynya, the fact that new freshly-refrozen leads appeared closer to the centre of the polynya area suggest that the ice opened again. In conclusion, the ice was very dynamic in 2017, with multiple openings and closing of leads potentially initiating the oceanic convection.

https://doi.org/10.5194/tc-2020-123
Preprint. Discussion started: 7 May 2020

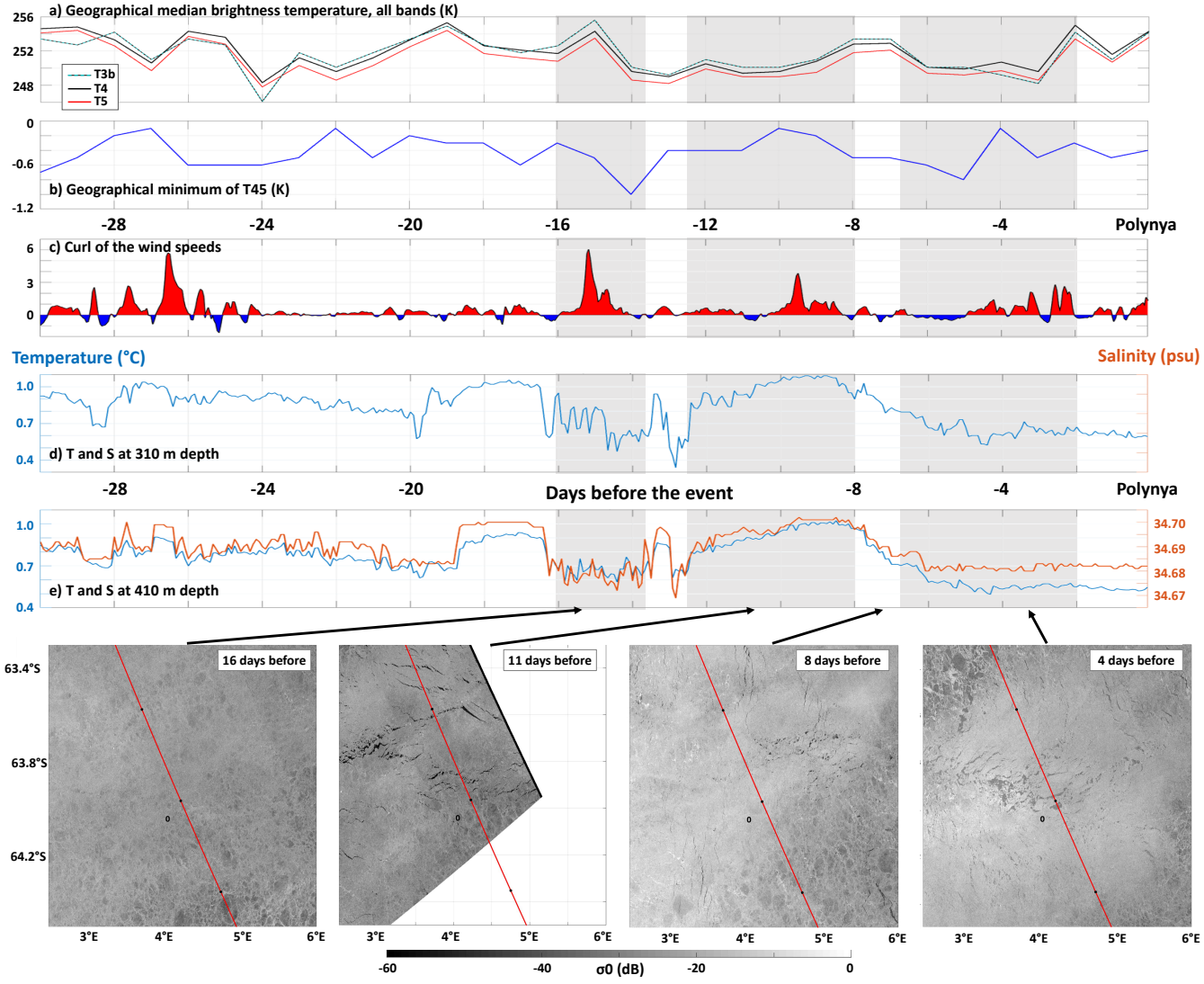

Figure 9. Conditions in the 30 days leading to the 3 September 2017 polynya. First, for the infrared criteria from section 3.2: a) geographical median over the polynya-prone region for the brightness temperature band T3b (cyan), T4 (thick black) and T5 (red); b) geographical min over the polynya-prone region of the brightness temperature difference T45 (T4 minus T5). c) curl of the wind speeds as in supp Fig. A4. Temperature (blue) and salinity (orange) timeseries from mooring 229-13 (see Fig. 6) at 310 (d), and 410 (e) m depth. Finally, Sentinel-1 images for four of these days, captured around 19 local time; observe the dark streaks made by leads. Red line indicates constant incidence angle; 0, the centre of the polynya region. Grey boxes in the background highlight the time periods discussed in the text. [Contains Sentinel-1 data, August-September 2017]

In summary, our results agree with both the oceanographic (von Schuckmann et al., 2019; Cheon and Gordon, 2019) and the atmospheric (Francis et al., 2019; Campbell et al., 2019) arguments. All three events that we could study in details show both

https://doi.org/10.5194/tc-2020-123
Preprint. Discussion started: 7 May 2020

upwelling and wind-induced leads. That is, the Maud Rise polynya presents the characteristics of both a sensible and latent heat polynya. Such a phenomenon has in fact been observed recently in a polynya off Alaska, and dubbed "hybrid polynya" (Hirano et al., 2016). Maybe it is time to admit that there has been no consensus in forty years because the Weddell Polynya is a hybrid polynya too.

4 Conclusions

The aim of this paper was to determine criteria on spaceborne infrared imagery (AVHRR / APP) to detect an upcoming reopening of the Weddell Polynya. Using the NSIDC sea ice concentration, we first generated a time series of past polynya events over Maud Rise and obtained 24 events since 1980, or 30 polynyas as some days had several polynyas opened simultaneously (Fig 2). The widely accepted narrative is that there had been no polynya in the Weddell Sea since "the" Weddell Polynya of 1974-1976 when the polynya unexpectedly re-opened in 2016 (e.g. Swart et al., 2018). Yet, our study is but one of many that found once again that there has in fact been many polynyas in the region in the forty years in between (e.g. Lindsay et al., 2004; Smedsrud, 2005; de Steur et al., 2007; Campbell et al., 2019).

Investigating the weeks leading to each of these 24 events, we found four criteria based on the area-average and area-maximum daily infrared brightness temperature in all bands that, when combined, successfully detected the events without finding false positives. Or rather, we thought it had returned 12 false positives, but a closer inspection (Table 1) revealed that these simply were smaller polynya events. The simplicity of this method, based on one data type, needing only one daily image, and scanning an entire region rather than looking for a moving point, means that it could easily be automated. The next step would be to check whether these criteria are still valid for other Antarctic open ocean polynyas such as the Cape Darnley Polynya (Ohshima et al., 2013), but also coastal polynyas (e.g. the Amundsen Sea Polynya Randall-Goodwin et al., 2015) or even Arctic polynyas (e.g. North Water and North Greenland polynyas, Preußer et al., 2015; Ludwig et al., 2019).

Finally, we investigated whether spaceborne infrared data could be used to answer the forty-year old debate: is it the ocean or the atmosphere that causes the Weddell Polynya to open? Using the infrared data combined with atmospheric reanalysis, mooring hydrographic time series and even Sentinel-1 SAR imagery, we found evidence of both (Figs. 7-9). We found obvious signatures of warm water upwelling and deep convection (e.g. Holland, 2001; Martin et al., 2013; Dufour, 2017; Cheon and Gordon, 2019) but also of wind-driven lead opening (e.g. Gordon et al., 2007; Cheon et al., 2014; Campbell et al., 2019; Francis et al., 2019). Our results suggest that there should not be any debate in fact: both parties are correct, and the Weddell Polynya probably is a hybrid one, as happens for some Arctic polynyas (Hirano et al., 2016).

This study also proved the crucial role of high resolution products. SAR imagery is widely used for lead detection in the Arctic (Murashkin et al., 2018), but as Sentinel satellites pass over the same spot only every 4 days at best, they are of limited use for operational purposes. We need more high resolution instruments in space, onboard more satellites. Moreover, this study would not have been possible without continuous observation programs, both in space (AVHRR) and at sea (moorings). These must be maintained, as long time series are crucial not just for statistical exercises like here, but also to monitor climate change in the fast-changing polar regions (Stocker et al., 2014).

https://doi.org/10.5194/tc-2020-123
Preprint. Discussion started: 7 May 2020

305 *Code availability.* Codes available on request

Data availability. Sea ice data freely available online at ftp://seaice.uni-bremen.de and https://nsidc.org/data/nsidc-0051. APP infrared data freely available at https://www.ncei.noaa.gov/data/avhrr-polar-pathfinder/access. ERA5 data freely available at https://cds.climate.copernicus.eu/cdsapp/dataset/reanalysis-era5-single-levels. Mooring data freely available on PANGAEA at https://doi.pangaea.de/10.1594/PANGAEA.[dataset numbers in reference list]. Sentinel-1 data freely available at https://scihub.copernicus.eu/

https://doi.org/10.5194/tc-2020-123
Preprint. Discussion started: 7 May 2020

The Cryosphere Discussions
Open Access
EGU

Table A1. Characteristics of the events detected in section 3.1, with sea ice concentration < 60% criterion: start date, latitude (lat., in degree North) and longitude (lon., in degree East) of the centre, maximum area (in km^2) and duration (in days).

Start date	centre lat.	centre lon.	max. area	duration
17 July 1980	-63.9	2.2	5625	3
15 July 1991	-64.1	4.7	12500	5
24 Oct 1991	-63.7	5.1	5000	8
23 Oct 1992	-63.8	5.4	25625	9
13 Aug 1994	-63.7	3.2	21875	6
20 Aug 1994	-63.9	4.2	7500	5
6 Sept 1994	-64.0	5.0	18125	15
18 Oct 1996	-63.4	5.6	9375	11
22 Oct 1996	-63.7	3.7	9375	7
	-63.6	6.6	625	1
30 Oct 1996	-63.4	5.6	625	1
27 July 1999	-67.7	-4.4	9375	1
	-66.6	-0.2	10000	2
24 Oct 1999	-66.4	-0.2	14375	8
29 Aug 2000	-66.4	-1.3	21875	3
27 Oct 2000	-65.1	1.0	1250	2
30 Oct 2000	-65.2	1.8	6875	2
	-64.2	6.8	14375	2
9 Oct 2004	-67.6	4.9	5000	4
	-63.8	5.7	8125	17
13 Oct 2004	-67.5	2.0	4375	2
	-66.6	5.6	7500	2
	-63.7	1.7	33125	14
9 Oct 2005	-63.9	2.2	1875	2
27 July 2016	-64.2	6.5	2500	3
31 July 2016	-64.1	5.7	625	1
2 Aug 2016	-64.3	6.3	43125	8
11 Aug 2016	-65.0	3.9	17500	4
3 Sept 2017	-63.9	3.7	3125	5
13 Sept 2017	-64.3	4.2	71875	49

https://doi.org/10.5194/tc-2020-123
Preprint. Discussion started: 7 May 2020

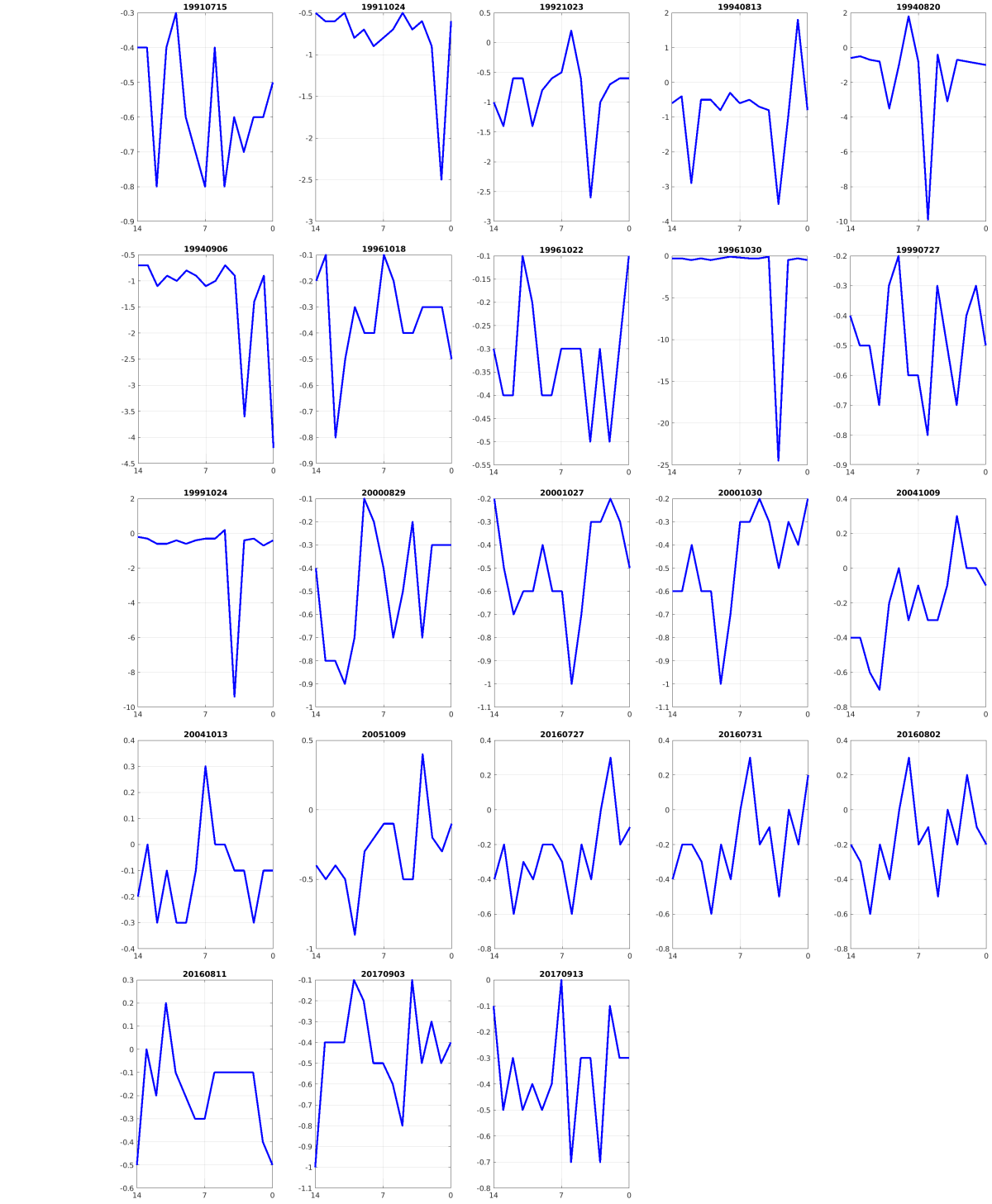

Figure A1. Time series of the geographical minimum brightness temperature difference T45 (T4 minus T5) over the 14 days leading to the polynya event (date of the event in the panel title). x-axis: Days before the polynya event; y-axis: temperature difference in K.

https://doi.org/10.5194/tc-2020-123
Preprint. Discussion started: 7 May 2020

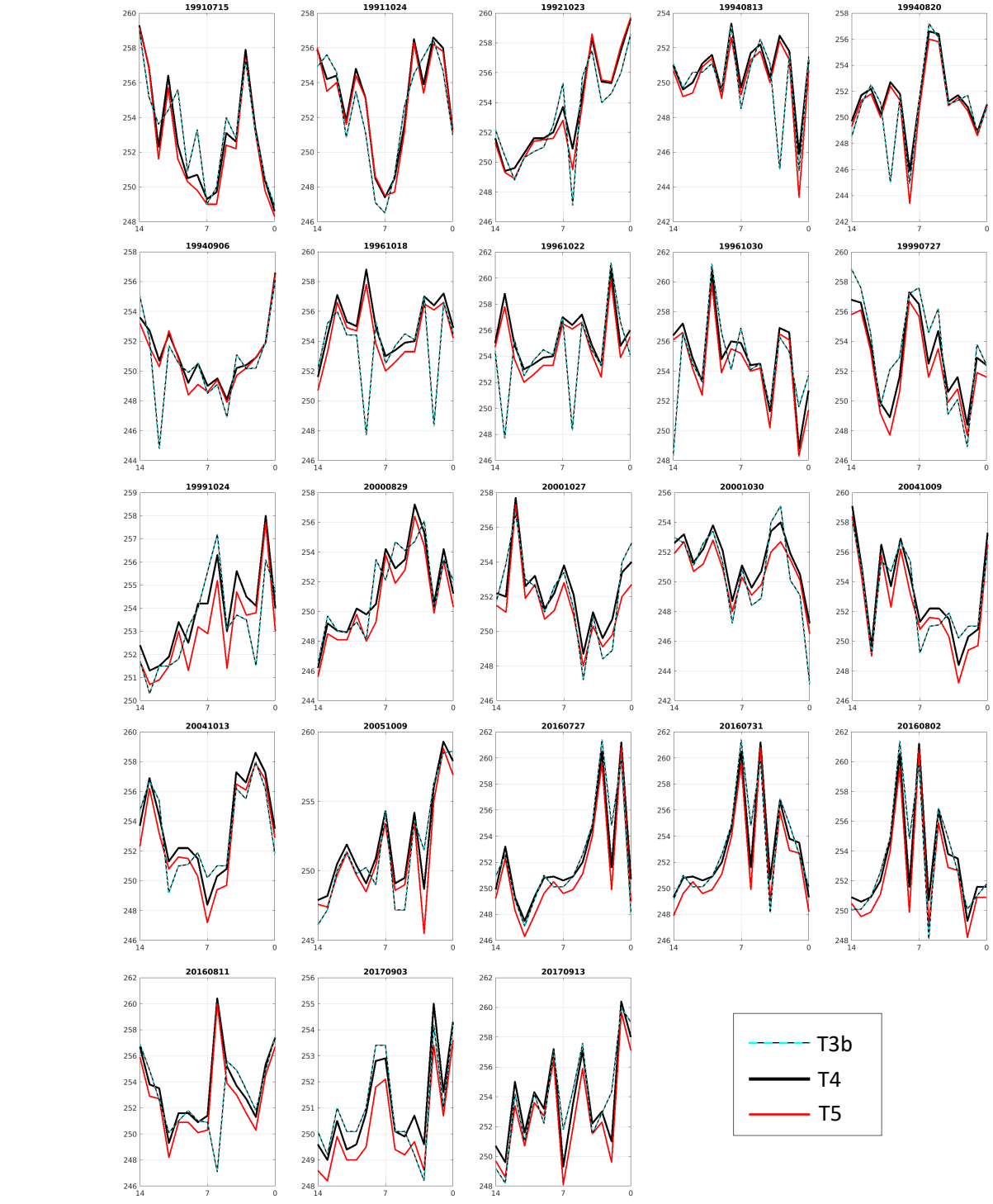

Figure A2. Time series of the geographical median brightness temperature for all three bands, over the 14 days leading to the polynya event (date of the event in the panel title). Thin dashed cyan line indicates T3b, thick black line T4, and red line T5. x-axis: Days before the polynya event; y-axis: temperature in K.

https://doi.org/10.5194/tc-2020-123
Preprint. Discussion started: 7 May 2020

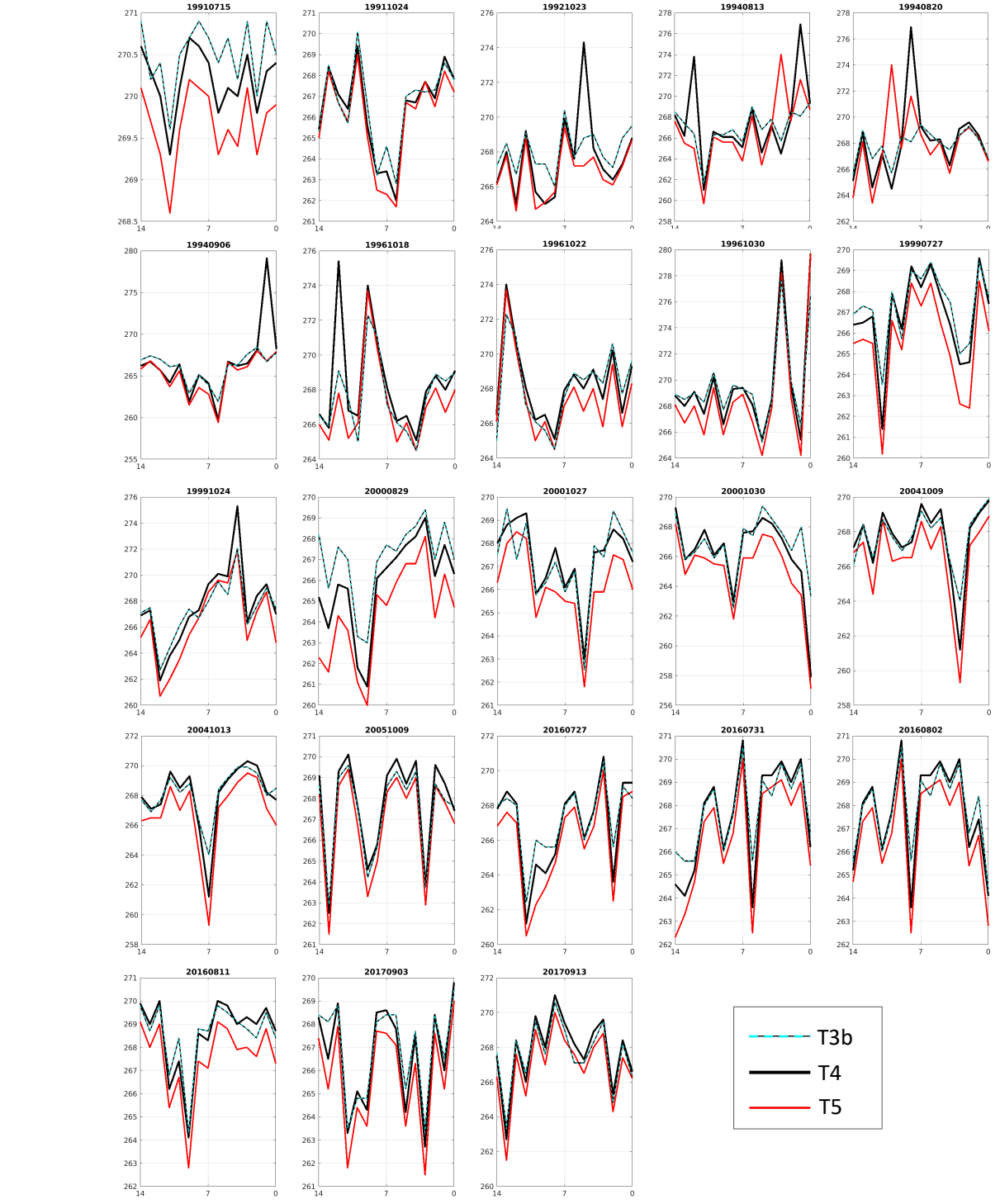

Figure A3. Time series of the geographical maximum brightness temperature for all three bands, over the 14 days leading to the polynya event (date of the event in the panel title). Thin dashed cyan line indicates T3b, thick black line T4, and red line T5. x-axis: Days before the polynya event; y-axis: temperature in K.

https://doi.org/10.5194/tc-2020-123
Preprint. Discussion started: 7 May 2020

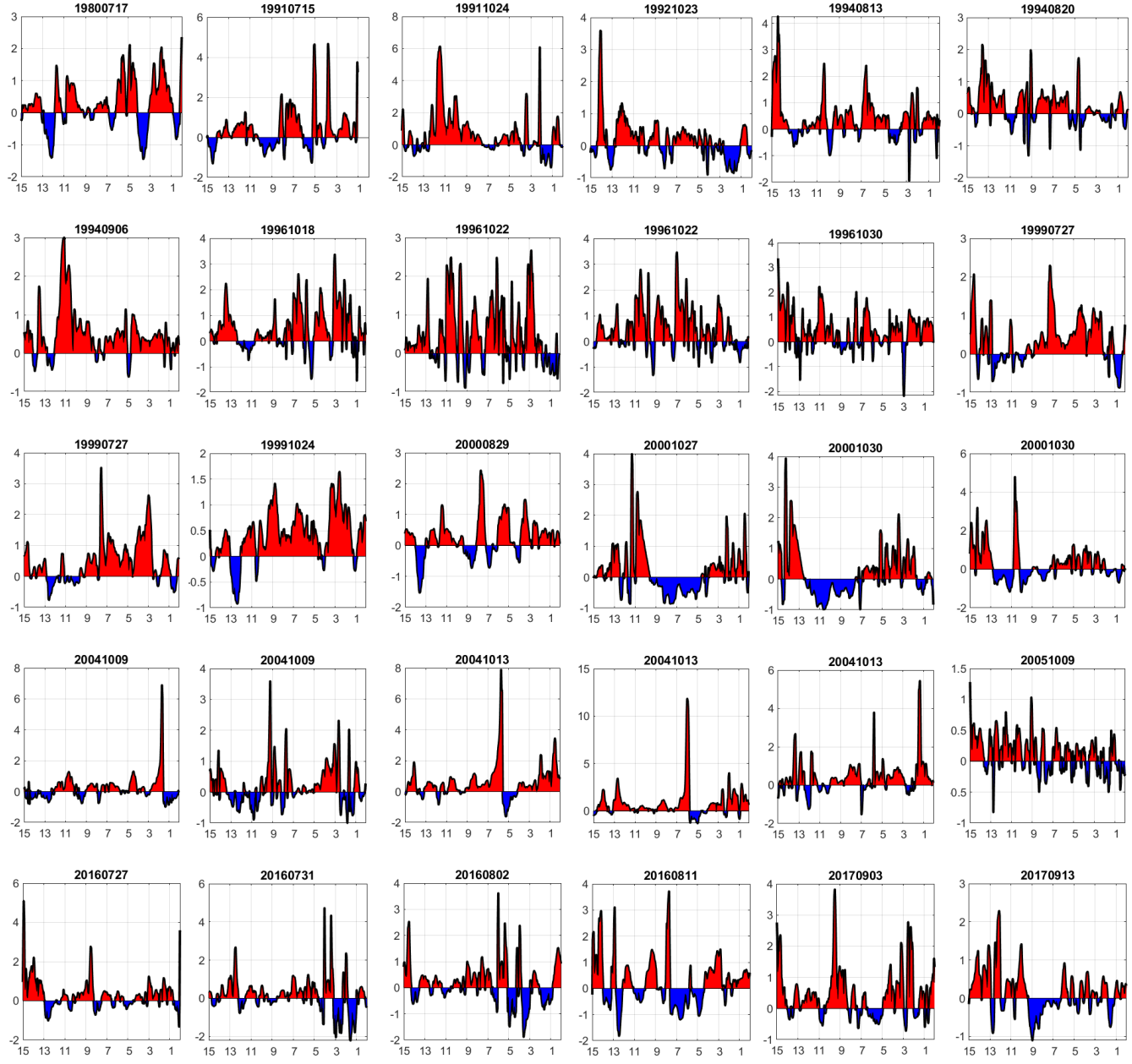

Figure A4. Time series of the curl of the wind at the location of the polynya, over the 15 days leading to the polynya event (date of the event in the panel title). x-axis: Days before the polynya event; y-axis: Curl of the wind as $\frac{\partial v}{\partial x} - \frac{\partial u}{\partial y}$, with the 10 m horizontal wind speeds u and v in ms^{-1} (see Methods).

https://doi.org/10.5194/tc-2020-123
Preprint. Discussion started: 7 May 2020

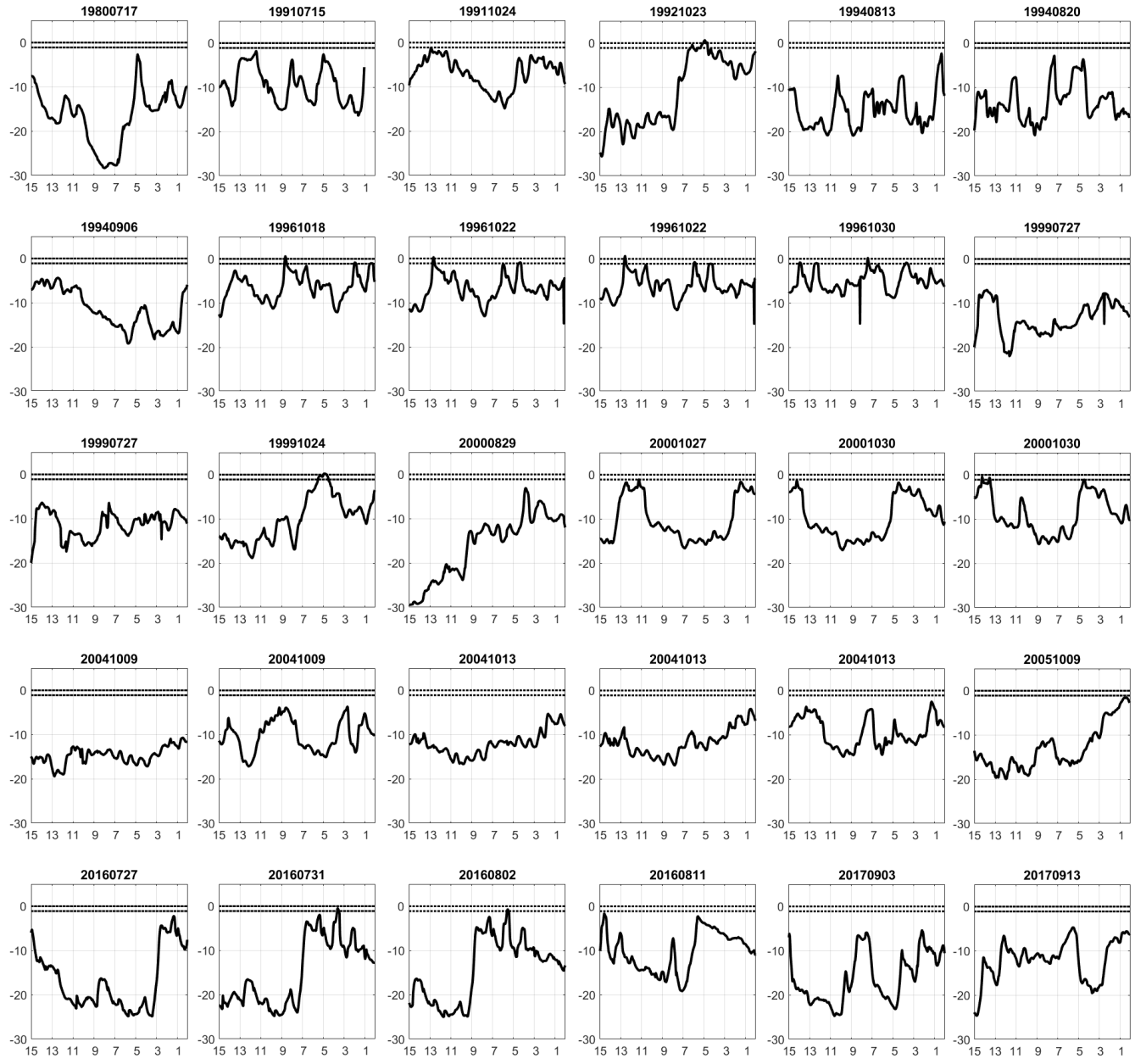

Figure A5. Time series of the 2 m air temperature at the location of the polynya, over the 15 days leading to the polynya event (date of the event in the panel title). x-axis: Days before the polynya event; y-axis: Air temperature in degree C. Horizontal dashed lines indicate the freezing temperature for young salty (-1.1 °C) or older fresh (0 °C) sea ice

https://doi.org/10.5194/tc-2020-123
Preprint. Discussion started: 7 May 2020

The Cryosphere
Discussions
Open Access
EGU

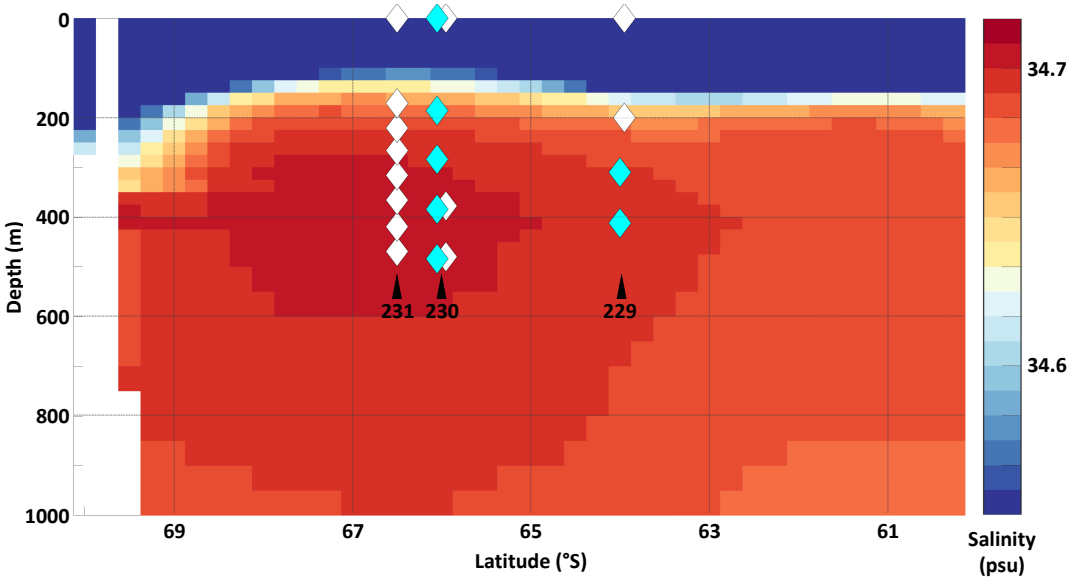

Figure A6. Climatological salinity along the Prime Meridian, from Zweng et al. (2018), showing the comparatively salty CDW in red. The diamonds indicate the location of the mooring sensors used for our analysis; for moorings 229 and 230, white indicates the older deployment (229-5, in 2002-2005, and 230-2, in 1999-2000) and cyan, the more recent one (229-13, in 2016-2019, and 230-4, 2002-2005); for mooring 231, only deployment 231-5 (2002-2005) could be used here.

https://doi.org/10.5194/tc-2020-123
Preprint. Discussion started: 7 May 2020

Author contributions. C.H. designed the study and conducted the Infrared and Mooring analysis. A.L. conducted the SAR analysis. Both authors contributed to the manuscript.

Competing interests. The authors declare no competing interest.

Acknowledgements. This project is funded by the Swedish National Space Agency (grant 164/18 awarded to C.H.). The authors thank Thomas Lavergne for his generous help while this idea was still at the proposal stage, and again, along with his colleagues at Metno, for their help with getting the data and eventually suggesting we use APP.

https://doi.org/10.5194/tc-2020-123
Preprint. Discussion started: 7 May 2020

References

Aldenhoff, W., C., H., and Eriksson, L.: Comparison of ice/water classification in Fram Strait from C-and L-band SAR imagery, Annals of Glaciology, 59, 112–123, 2018.

Campbell, E., Wilson, E. A., Moore, G., Riser, S., Brayton, C. E., Mazloff, M., and Talley, L.: Antarctic offshore polynyas linked to Southern Hemisphere climate anomalies, Nature, 570, 319–325, 2019.

Carsey, F.: Microwave observation of the Weddell Polynya, Monthly Weather Review, 108, 2032–2044, 1980.

Cavalieri, D., Parkinson, C., Gloersen, P., and Zwally, H.: Sea Ice Concentrations from Nimbus-7 SMMR and DMSP SSM/I-SSMIS Passive Microwave Data, Version 3.1, Boulder, Colorado USA. NASA National Snow and Ice Data Center Distributed Active Archive Center, https://doi.org/10.5067/8GQ8LZQVL0VL, last accessed 8 November 2019, 1996.

Cheon, W. and Gordon, A.: Open–ocean polynyas and deep convection in the Southern Ocean, Scientific reports, 9, 1–9, 2019.

Cheon, W., Park, Y., Toggweiler, J., and Lee, S.: The relationship of Weddell Polynya and open-ocean deep convection to the Southern Hemisphere westerlies, Journal of physical oceanography, 44, 694–713, 2014.

Comiso, J.: Satellite remote sensing of the Polar Oceans, Journal of Marine Systems, 2, 395–434, 1991.

de Steur, L., Holland, D., Muench, R., and McPhee, M.: The warm-water "Halo" around Maud Rise: Properties, dynamics and impact, Deep Sea Research Part I: Oceanographic Research Papers, 54, 871–896, 2007.

Demchev, D., Volkov, V., Kazakov, E., Alcantarilla, P. F., Sandven, S., and Khmeleva, V.: Sea ice drift tracking from sequential SAR images using accelerated-KAZE features, IEEE Transactions on Geoscience and Remote Sensing, 55, 5174–5184, 2017.

Drinkwater, M.: Satellite microwave radar observations of Antarctic sea ice. In Analysis of SAR data of the polar oceans, Springer, 1998.

Dufour, C. O., M. A. K. G. S. M. F. I. Z. H. . W. M.: Preconditioning of the Weddell Sea polynya by the ocean mesoscale and dense water overflows, Journal of Climate, 30, 7719–7737, 2017.

Fahrbach, E. and Rohardt, G.: Physical oceanography and current meter data from mooring AWI229-5, Alfred Wegener Institute, Helmholtz Centre for Polar and Marine Research, Bremerhaven, PANGAEA, https://doi.org/10.1594/PANGAEA.793018, 2012a.

Fahrbach, E. and Rohardt, G.: Physical oceanography and current meter data from mooring AWI230-2, Alfred Wegener Institute, Helmholtz Centre for Polar and Marine Research, Bremerhaven, PANGAEA, https://doi.org/10.1594/PANGAEA.793080, 2012b.

Fahrbach, E. and Rohardt, G.: Physical oceanography and current meter data from mooring AWI230-4, Alfred Wegener Institute, Helmholtz Centre for Polar and Marine Research, Bremerhaven, PANGAEA, https://doi.org/10.1594/PANGAEA.793082, 2012c.

Fahrbach, E. and Rohardt, G.: Physical oceanography and current meter data from mooring AWI231-5, Alfred Wegener Institute, Helmholtz Centre for Polar and Marine Research, Bremerhaven, PANGAEA, https://doi.org/10.1594/PANGAEA.793089, 2012d.

Francis, D., Eayrs, C., Cuesta, J., and Holland, D.: Polar cyclones at the origin of the reoccurrence of the Maud Rise Polynya in austral winter 2017, Journal of Geophysical Research: Atmospheres, 124, 5251–5267, 2019.

GEBCO Compilation Group: GEBCO 2019 Grid, https://doi.org/10.5285/836f016a-33be-6ddc-e053-6c86abc0788e, 2019.

Gloersen, P., Campbell, W., Cavalieri, D., Comiso, J., Parkinson, C., and Zwally, H.: Arctic and Antarctic sea ice, 1978–1987, Satellite Passive-Microwave Observations and Analysis, 290, 1992.

Gordon, A.: Deep Antarctic convection west of Maud Rise, Journal of Physical Oceanography, 8, 600–612, 1978.

Gordon, A., Visbeck, M., and Comiso, J.: A possible link between the Weddell Polynya and the Southern Annular Mode, Journal of Climate, 20, 2558–2571, 2007.

https://doi.org/10.5194/tc-2020-123
Preprint. Discussion started: 7 May 2020

Heuzé, C. and Aldenhoff, W.: Near-Real Time Detection of the Re-Opening of the Weddell Polynya, Antarctica, from Spaceborne Infrared Imagery, IGARSS 2018-2018 IEEE International Geoscience and Remote Sensing Symposium, pp. 5613–5616, 2018.

Heuzé, C., Heywood, K., Stevens, D., and Ridley, J.: Changes in global ocean bottom properties and volume transports in CMIP5 models under climate change scenarios, Journal of Climate, 28, 2917–2944, 2015a.

Heuzé, C., Ridley, J., Calvert, D., Stevens, D., and Heywood, K.: Increasing vertical mixing to reduce Southern Ocean deep convection in NEMO3.4, Geoscientific Model Development, 8, 3119–3130, 2015b.

Hirano, D., Fukamachi, Y., Watanabe, E., Ohshima, K., Iwamoto, K., Mahoney, A., Eicken, H., Simizu, S., and Tamura, T.: A wind-driven, hybrid latent and sensible heat coastal polynya off Barrow, Alaska, Journal of Geophysical Research: Oceans, 121, 980–997, 2016.

Holland, D. M.: Explaining the Weddell Polynya–a large ocean eddy shed at Maud Rise, Science, 292, 1697–1700, 2001.

IOC, SCOR and IAPSO: The international thermodynamic equation of seawater - 2010: Calculation and use of thermodynamic properties, Tech. rep., UNESCO, available from http://www.TEOS-10.org, 2010.

Key, J. and Barry, R.: Cloud cover analysis with Arctic AVHRR data: 1. Cloud detection, Journal of Geophysical Research: Atmospheres, 94, 18 521–18 535, 1989.

Key, J., Liu, Y., Wang, X., and NOAA CDR Program: NOAA Climate Data Record (CDR) of AVHRR Polar Pathfinder (APP) Cryosphere, Version 2.0, NOAA National Centers for Environmental Information (NCEI), https://doi.org/10.25921/X2X1-JR34, last accessed 15 January 2020, 2019.

Kjellsson, J., Holland, P., Marshall, G., Mathiot, P., Aksenov, Y., Coward, A., Bacon, S., Megann, A., and Ridley, J.: Model sensitivity of the Weddell and Ross seas, Antarctica, to vertical mixing and freshwater forcing, Ocean Modelling, 94, 141–152, 2015.

Korosov, A., Rampal, P., Toudal Pedersen, L., Saldo, R., Ye, Y., Heygster, G., Lavergne, T., Aaboe, S., and Girard Ardhuin, F.: A new tracking algorithm for sea ice age distribution estimation, The Cryosphere, 12, 2073–2085, 2018.

Lindsay, R., Holland, D., and Woodgate, R.: Halo of low ice concentration observed over the Maud Rise seamount, Geophysical research letters, 31, 2004.

Locarnini, R., Mishonov, A., Baranova, O., Boyer, T., Zweng, M., Garcia, H., Reagan, J., Seidov, D., Weathers, K., Paver, C., and Smolyar, I.: World Ocean Atlas 2018, Volume 1: Temperature, A. Mishonov Technical Ed.; NOAA Atlas NESDIS 81, 2018.

Ludwig, V., Spreen, G., Haas, C., Istomina, L., Kauker, F., and Murashkin, D.: The 2018 North Greenland polynya observed by a newly introduced merged optical and passive microwave sea-ice concentration dataset, The Cryosphere, 13, 2019.

Mäkynen, M., Kern, S., Rösel, A., and Pedersen, L.: On the estimation of melt pond fraction on the Arctic Sea ice with ENVISAT WSM images, IEEE Transactions on Geoscience and Remote Sensing, 52, 7366–7379, 2014.

Martin, S. and Cavalieri, D.: Contributions of the Siberian shelf polynyas to the Arctic Ocean intermediate and deep water, Journal of Geophysical Research: Oceans, 94, 12 725–12 738, 1989.

Martin, T., Park, W., and Latif, M.: Multi-centennial variability controlled by Southern Ocean convection in the Kiel Climate Model, Climate dynamics, 40, 2005–2022, 2013.

Meier et al., W.: Arctic sea ice in transformation: A review of recent observed changes and impacts on biology and human activity, Reviews of Geophysics, 52, 185–217, 2014.

Morales Maqueda, M., Willmott, A., and Biggs, N.: Polynya dynamics: A review of observations and modeling, Reviews of Geophysics, 42, 2004.

Murashkin, D., Spreen, G., Huntemann, M., and Dierking, W.: Method for detection of leads from Sentinel-1 SAR images, Annals of Glaciology, 59, 124–136, 2018.

https://doi.org/10.5194/tc-2020-123
Preprint. Discussion started: 7 May 2020

Nandan, V., Geldsetzer, T., Yackel, J., Mahmud, M., Scharien, R., Howell, S., King, J., Ricker, R., and Else, B.: Effect of snow salinity on CryoSat-2 Arctic first-year sea ice freeboard measurement, Geophysical Research Letter, 44, 10–419, 2017.

Notz, D. and Stroeve, J.: Observed Arctic sea-ice loss directly follows anthropogenic CO2 emission, Science, 354, 747–750, 2016.

Ohshima et al., K.: Antarctic Bottom Water production by intense sea-ice formation in the Cape Darnley polynya, Nature Geoscience, 6, 235–240, 2013.

Petty, A., Hutchings, J., Richter-Menge, J., and Tschudi, M.: Sea ice circulation around the Beaufort Gyre: The changing role of wind forcing and the sea ice state, Journal of Geophysical Research: Oceans, 121, 3278–3296, 2016.

Preußer, A., Heinemann, G., Willmes, S., and Paul, S.: Sea ice circulation around the Beaufort Gyre: The changing role of wind forcing and the sea ice state, Multi-decadal variability of polynya characteristics and ice production in the North Water Polynya by means of passive microwave and thermal infrared satellite imagery, 7, 15 844–15 867, 2015.

Randall-Goodwin, E., Meredith, M., Jenkins, A., Y. P., Sherrell, R., Abrahamsen, E., Guerrero, R., Yuan, X., Mortlock, R., Gavahan, K., and Alderkamp, A.: Freshwater distributions and water mass structure in the Amundsen Sea Polynya region, Antarctica, Elementa: Science of the Anthropocene, 3, 2015.

Rohardt, G. and Boebel, O.: Physical oceanography and current meter data from mooring AWI229-13, Alfred Wegener Institute, Helmholtz Centre for Polar and Marine Research, Bremerhaven, PANGAEA, https://doi.org/10.1594/PANGAEA.898781, 2019.

Saunders, R. W. and Kriebel, K. T.: An improved method for detecting clear sky and cloudy radiances from AVHRR data, International Journal of Remote Sensing, 9, 123–150, 1988.

Schillat, M., Jensen, M., Vereda, M., Sánchez, R. A., and Roura, R.: Tourism in Antarctica: A multidisciplinary view of new activities carried out on the white continent, Springer, 2016.

Smedsrud, L.: Warming of the deep water in the Weddell Sea along the Greenwich meridian: 1977–2001, Deep Sea Research Part I: Oceanographic Research Papers, 52, 241–258, 2005.

Smith Jr, W. O., , and Barber, D.: Polynyas: Windows to the world, Elsevier, 2007.

Spreen, G., Kaleschke, L., and Heygster, G.: Sea ice remote sensing using AMSR-E 89-GHz channels , Journal of Geophysical Research: Oceans, 113, 2008.

Stocker et al., T. F.: Climate change 2013: the physical science basis. Contribution of working group I to the fifth assessment report of IPCC the intergovernmental panel on climate change, Cambridge University Press, 2014.

Swart et al., S.: Return of the Maud Rise polynya: Climate litmus or seaice anomaly? [in"State of the Climate in 2017"], Bulletin of the American Meteorological Society, 99, S188–S189, 2018.

Vincent, R., Marsden, R., Minnett, P., and Buckley, J.: Arctic waters and marginal ice zones: 2. An investigation of arctic atmospheric infrared absorption for advanced very high resolution radiometer sea surface temperature estimates, Journal of Geophysical Research: Oceans, 113, 2008.

von Schuckmann et al., K.: Copernicus Marine Service Ocean State Report, Issue 3, Journal of Operational Oceanography, 12, S1–S123, 2019.

Wilson, E., Riser, S., Campbell, E. C., and Wong, A.: Winter upper-ocean stability and ice–ocean feedbacks in the sea ice–covered Southern Ocean, Journal of Physical Oceanography, 49, 1099–1117, 2019.

Yamanouchi, T., Suzuki, K., and Kawaguchi, S.: Detection of clouds in Antarctica from infrared multispectral data of AVHRR, Journal of the Meteorological Society of Japan. Ser. II, 65, 949–962, 1987.

https://doi.org/10.5194/tc-2020-123
Preprint. Discussion started: 7 May 2020

Zanowski, H., Hallberg, R., and Sarmiento, J.: Abyssal ocean warming and salinification after Weddell polynyas in the GFDL CM2G coupled climate model, Journal of Physical Oceanography, 45, 2755–2772, 2015.

Zhang, X., Dierking, W., Zhang, J., Meng, J., and Lang, H.: Retrieval of the thickness of undeformed sea ice from simulated C-band compact polarimetric SAR images, The Cryosphere, 10, 1529–1545, 2016.

Zweng, M., Reagan, J., Seidov, D., Boyer, T., Locarnini, R., Garcia, H., Mishonov, A., Baranova, O., Weathers, K., Paver, C., and Smolyar, I.: World Ocean Atlas 2018, Volume 2: Salinity, A. Mishonov Technical Ed.; NOAA Atlas NESDIS 82, 2018.